Russian Journal of Earth Sciences Online ISSN: 1681-1208

On the Choice of Tidal Forcing at the Open Boundaries in a High-Resolution Regional Kara Sea Model

S. D. Martyanov*,[1], A. Y. Dvornikov[1], D. V. Sein[1,2], and V. A. Gorchakov[1]

[1] Shirshov Institute of Oceanology, Russian Academy of Sciences, Moscow, Russian Federation
[2] Alfred Wegener Institute, Helmholtz Centre for Polar and Marine Research, Bremerhaven, Germany
* **Correspondence to:** Stanislav Martyanov, martyanov.sd@gmail.com

Abstract: Tidal dynamics play an important role in Kara Sea circulation, influencing currents, sea ice formation, and biogeochemical processes. However, accurate numerical simulation of these processes in regional models depends on the choice of tidal forcing at open lateral boundaries. This study evaluates the performance of three tidal models – TPXO9, FES2014, and Arc2kmTM as sources of boundary forcing for a high-resolution regional Kara Sea model based on MITgcm numerical kernel. The goal is to identify the optimal tidal forcing that best aligns with observations from coastal stations. Numerical experiments have revealed significant discrepancies in tidal energy estimates among the models. The FES2014 model has shown the closest agreement to observations, while Arc2kmTM exhibits the largest errors. However, when used as boundary forcing in the regional Kara Sea model, Arc2kmTM yields the smallest errors in simulated tidal amplitude and phase. Overall, the regional model reproduces M2 tidal amplitudes well but introduces slight phase shifts in the southwestern part of the Kara Sea. Our findings emphasize that no single tidal model can be considered universally optimal. The choice depends on regional conditions and modeling objectives. For our regional model, Arc2kmTM is recommended as a source of tidal forcing at the open boundaries of the regional model, though global models like FES2014 remain viable alternatives. This work emphasizes the need for improved validation methods and highlights the challenges posed by limited observational data in the Arctic region.

Keywords: Kara Sea, tide, numerical modeling, tidal forcing, open boundary

Citation: Martyanov S. D., Dvornikov A. Y., Sein D. V., and Gorchakov V. A. (2026), On the Choice of Tidal Forcing at the Open Boundaries in a High-Resolution Regional Kara Sea Model, *Russian Journal of Earth Sciences*, 26, ES1021, EDN: NPDXNU, https://doi.org/10.2205/2026es001080

1. Introduction

Tidal movements play an important role in ocean dynamics, but their impact is especially pronounced in shelf and coastal areas where the tidal mode of movement can become dominant in some cases. Accounting for tidal movements is important for solving various problems of shipping, building of hydrotechnical structures, oil and gas mining, etc. More generally, it is important from the point of view of the fundamental study of processes occurring in the World Ocean. In the Arctic region, accounting for tidal movements is also important due to the presence of specific conditions, such as the relative shallowness of the ocean, an extensive shelf area, the presence of sea ice, and considerable river runoff. Although accounting for tidal dynamics does not significantly affect the overall extent of sea ice in the Arctic shelf seas, [*Postlethwaite et al.*, 2011] demonstrated that in coastal areas with a pronounced tidal impact to the resultant current it delays freezing and accelerates the onset of sea ice melting because tidal vertical mixing can increase the heat flux from deeper water masses to the surface.

The structure of tidal oscillations in the Kara Sea was studied using in situ measurement data by [*Voinov and Naumov*, 2017] for the southwestern part of the sea near Vaygach Island, by [*Voinov et al.*, 2020] for the southern part of the sea near Bely Island, as well as in a series of works [e.g., *Voinov et al.*, 2023; *Voinov and Piskun*, 2019, 2023] focused on

Research Article

Received: April 8, 2025
Accepted: November 5, 2025
Published: April 28, 2026

the study of tidal oscillations in the Gulf of Ob. Besides, it was shown that the impact of tidal dynamics on the structure of hydrophysical fields in the Kara Gate Strait significantly affects the characteristics of internal waves and their interaction with the mean flow, as was reported by [*Morozov et al.*, 2017, 2008] who used in situ and satellite measurements for their analysis. [*Li et al.*, 2019] also studied internal waves in that region, but using a non-hydrostatic numerical model, and their results helped clarify the structure and evolution of internal waves in the strait.

In most cases, field observations of tidal oscillations represent sea level data measured at coastal gauges or individual locations in the open sea. Using such data, it is possible to perform a detailed analysis of tidal movements' structure at a given point and its vicinity, but, unfortunately, such conclusions cannot be freely generalized to a more extended area, be it the entire marginal sea or some part of it, a large bay or more distant points of the coastline. In this case there is a need to use mathematical models that take into account physical and geographical features of an object under study such as its position, depth field, coastline configuration, hydrophysical properties, etc. These models simulate the state of the environment using a system of equations describing dynamic, thermodynamic, and other processes, such as biogeochemical, lithodynamic, or any other, depending on the particular goals of a study. Despite the fact that tidal dynamics can be described with a relatively good accuracy by two-dimensional models in many cases, at present it is advisable to use a three-dimensional formulation for a full description of the process. For example, [*Cai et al.*, 2006] showed that taking into account the three-dimensionality of the process (in comparison with a two-dimensional formulation), density stratification, atmospheric forcing, and adequate open boundary conditions for tidal forcing significantly improved the results of sea level simulation in the South China Sea, which is confirmed by a comparison with measurements at coastal stations. This conclusion is generally valid for other shelf areas and marginal seas.

When studying tidal dynamics using regional numerical models, the specification of open boundary conditions plays a crucial role. To date, open boundary conditions in such studies are specified using either sea level and current velocity values with sufficient temporal discretization, or in the form of spectral characteristics of tidal harmonics when the tidal component is filtered out from an external solution and specified separately. For instance, [*Janeković and Powell*, 2012] compared the results of tidal dynamics simulation under idealized and realistic conditions using two different methods for tidal forcing specification at the open boundaries. In the first case, tidal forcing taken from an external model solution was specified at the open boundaries along with all other state variables with a required discretization. In the second case, the tidal component had been pre-filtered from the external solution and was specified separately at the open boundaries as spectral forcing using phases and amplitudes of tidal oscillations. Numerical experiments showed that specifying tidal forcing in the second case significantly improved the model solution, whereas in the first case, due to insufficient discretization of tidal forcing at the open boundaries, there was a reduction in amplitude magnitudes and aliasing of tidal energy at high frequencies. It was also noted that when specifying not only one but multiple tidal harmonics, the above-mentioned problems would increase due to nonlinear interactions. Similar conclusions were reported by [*Solano et al.*, 2020] who used a high-resolution regional numerical model. Overall, it can be summarized that specification of the adequate open boundary conditions in regional ocean models still remains a challenging task and requires careful attention in each specific case, although several successful methodologies have been proposed earlier [e.g., *Marchesiello et al.*, 2001; *Mason et al.*, 2010].

[*Harms*, 1992] carried out one of the first simulations of the Kara Sea circulation using a three-dimensional regional model with a rather coarse spatial resolution equal to about 18 km where the contribution of the tidal component to the overall circulation of the Kara Sea was assessed, and a tidal map of the M2 wave was proposed based on numerical modeling. Tidal forcing at the open boundaries in those simulations was specified in the form of amplitudes and phases of the M2 wave taken from an external tidal model of the

Arctic Ocean. Despite a relatively coarse spatial resolution and significant limitations of the model, the study managed to obtain the correct positions of amphidromic points and the distribution of M2 wave phases across the sea. More recently, dynamics and characteristics of tidal motions in the Kara Sea were extensively investigated in a series of studies reported by the research group from the Shirshov Institute of Oceanology [e.g., *Kagan et al.*, 2019; *Kagan and Timofeev*, 2017] using the regional model based on QUODDY-4. They simulated the M2 tidal wave and its potential impact on mixing and regional climate in the Kara Sea. In their model runs, the amplitude and phase of the M2 wave were taken from the Arctic Ocean tidal model [*Padman and Erofeeva*, 2004] and specified at the open boundaries of the domain. The intra-annual variability of hydrophysical characteristics in the Gulf of Ob, and the interaction of primary production and sea ice in the Kara Sea were investigated by [*Chantsev and Danshina*, 2019] and [*Martyanov et al.*, 2018], respectively. In both studies the authors used modern high-resolution regional models based on Delft3D and MITgcm, each of them taking into account tidal motion, which was the primary mode of motion in the former study.

Currently, several different sources can be used to specify tidal forcing at the open boundaries of regional models of the Arctic Ocean marginal seas. Among the most popular are the products of tidal models TPXO9 [*Egbert and Erofeeva*, 2002], FES2014 [*Lyard et al.*, 2021], and Arc2kmTM [*Howard and Padman*, 2021]. However, although these products are obtained using modern hydrodynamic models and data assimilation techniques, their simulation results for the Kara Sea are not identical. This is quite understandable due to a possible use of different bathymetric data, spatial resolutions, and implementation features. At the same time, from the perspective of obtaining the most accurate results in a specific Kara Sea regional model, it becomes important to determine which tidal forcing at the open boundaries provides a numerical solution that most closely matches the real tidal oscillations and best agrees with observation data. For example, similar tasks were addressed in the study reported by [*Nguyen and Lee*, 2020] for the Yellow Sea and by [*Romanenkov et al.*, 2023] for the coastal region off the Kamchatka Peninsula. It was found in both studies that the internal solutions of regional numerical models were weakly dependent on the choice of tidal forcing at the open boundaries. However, it was also shown that coarse-resolution parent tidal models, from which the tidal boundary conditions for regional models had been taken, could provide a highly distorted description of tidal dynamics in the coastal zone and their solutions could significantly differ from each other, while more detailed regional models provided a substantially better description of tidal processes. In this regard, it seems important to carry out a similar analysis for the Kara Sea using a high-resolution numerical model to determine the optimal tidal forcing necessary for the correct simulation of tidal dynamics in this region, which is the main goal of the current study.

2. Data and Methods

2.1. Observation Data

Sources of tidal observation data in the Arctic seas of Russia are rather scarce and based mainly on information obtained during the Soviet era. First of all, these are harmonic constants for predicting the tidal sea level elevation taken from tide tables issued in various years by Soviet and non-Soviet hydrographic services. There also exist data on the tidal sea level in the Arctic seas obtained at long-term observation stations and published in 1994 [*Kowalik and Proshutinsky*, 2013]. More recently, the Arctic Tidal Constituents Atlas (ArcTiCA) became freely available [*Hart-Davis et al.*, 2024]. This product combines the analysis of in situ sea level measurements at coastal tidal gauges, bottom pressure sensors data and those obtained using reflectometry data. We also have at our disposal the tables of the Hydrographic Office of the USSR Navy and the Admiralty tide tables of the Hydrographic Office of the United Kingdom. After cross-checking of the combined information and removing duplicates, our database of tidal harmonic constants for the Kara Sea includes 31 observation points (Figure 1).

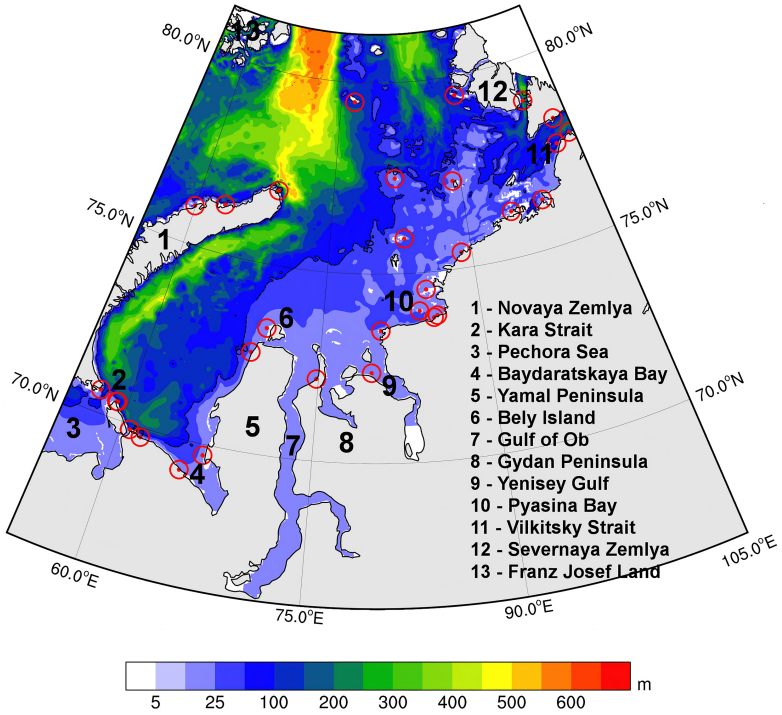

Figure 1. Bathymetry of the Kara Sea based on the GEBCO 2019 data. Red circles show the location of tide gauges used in our analysis.

2.2. External Tidal Models

The most popular global tidal models to date are the Oregon State University TOPEX/Poseidon Global Inverse Solution tidal model – TPXO [*Egbert and Erofeeva*, 2002] and the latest finite element solution global ocean tidal atlas – FES2014 [*Lyard et al.*, 2021]. Global solutions based on these systems (TPXO9 (version 4) and FES2024, respectively) are often used to define and specify tide-related information at the open lateral boundaries of regional ocean models. The TPXO9 atlas has a spatial resolution of 1/30° and is based on a global barotropic tidal model that uses assimilation procedures of satellite and tidal buoy data. The archive includes harmonic constants (amplitudes and phases of tidal sea level oscillations and components of barotropic tidal currents) for 15 tidal components, namely M2, S2, N2, K2, K1, O1, P1, Q1, Mf, Mm, M4, MS4, MN4, 2N2, S1. The FES2014 atlas is a global product created on the basis of a finite element barotropic tidal model with spatial resolution equal to 2–60 km depending on the local depth. The FES2014 tidal model uses assimilation of satellite and in situ observations. Available FES2014 data are presented on a grid with a spatial resolution of 1/16° for 34 tidal harmonics.

We also use the data from the most detailed regional tidal model to date – Arctic 2-kilometer Tide Model (Arc2kmTM). It was developed at the Earth and Space Research Institute in collaboration with Oregon State University in 2021 [*Howard and Padman*, 2021]. Arc2kmTM is a regional barotropic tidal model of the Arctic Ocean implemented on a grid with a spatial resolution of 2 km and based on the Regional Ocean Modeling System numerical kernel. Arc2kmTM provides sea surface height and depth-integrated current velocity for 8 tidal components (M2, S2, K1, O1, N2, P1, K2, Q1). The bathymetry of the model is based on the International Bathymetric Chart of the Arctic Ocean (IBCAO) version 3.0 [*Jakobsson et al.*, 2012]. Being a regional model, Arc2kmTM uses tidal current velocities and sea level heights taken from the TOPEX/Poseidon global barotropic tidal model at the open lateral boundaries.

2.3. Regional Kara Sea Model

A regional implementation of a three-dimensional Massachusetts Institute of Technology general circulation model – MITgcm [*Marshall et al.*, 1997], specifically adopted and configured for the Kara Sea conditions, is used in this study. A detailed description of the model was reported by [*Martyanov*, 2023], therefore we only provide main features of the model here in order to outline the physics and numerical aspects it incorporates. MITgcm solves the Boussinesq form of the Navier-Stokes equations for an incompressible fluid in a curvilinear framework. The model equations are written in z-coordinates and discretized using a staggered Arakawa C-grid. Water temperature and salinity are calculated using an advection-diffusion equation with corresponding boundary conditions. The water density is calculated using a modified UNESCO equation of state proposed in [*Jackett and McDougall*, 1995]. MITgcm is coupled with a sea-ice model described in [*Losch et al.*, 2010]. The model's domain is shown in Figure 1. This high-resolution regional numerical model of the Kara Sea (KASM) is run in a hydrostatic mode and utilizes the following set of main features. Vertical mixing in the model is parameterized with the TKE closure scheme proposed by [*Gaspar et al.*, 1990], horizontal turbulent mixing uses the modified Leith viscosity parametrization [*Leith*, 1996]. Time-stepping uses the Crank-Nicolson scheme for the sake of better energy conservation [*Campin et al.*, 2004], while a tracer advection scheme is a third-order direct space-time method with a flux limiter.

The KASM's grid consists of 1000×1100 cells horizontally and 50 unevenly distributed z-levels vertically. The horizontal resolution of the model is about 1530 m along meridians and 850–2264 m along parallels, the effective horizontal resolution being approximately 1500 m in the center of the domain, thus making the model eddy-resolving almost everywhere throughout the domain [*Hallberg*, 2013; *Nurser and Bacon*, 2014]. This configuration is more advantageous over those used in our earlier studies focused on modeling of the arctic seas' dynamics and biogeochemistry [e.g., *Martyanov et al.*, 2017, 2018] due to a better simulation of eddy dynamics and their impact on circulation and other processes achieved by resolving the first baroclinic deformation radius in the domain explicitly. The vertical resolution of KASM is 2–5 meters in the upper layers and reaches 30–50 meters in the deepest parts of troughs.

The depth field is taken from the GEBCO 2019 bathymetry database [*Jakobsson et al.*, 2012]. A no-slip and impermeability conditions are used for the solid boundaries. A parametrization proposed by [*Parkinson and Washington*, 1979] is applied for respective fluxes at the ocean-atmosphere interface. Initial conditions, as well as boundary values for water temperature, salinity, non-tidal current velocity, and sea-ice characteristics are taken from the daily-mean data provided by the global oceanic and sea ice reanalysis GLORYS12 [*Jean-Michel et al.*, 2021]. At the open lateral boundaries, we use a Dirichlet-type condition combined with a nudging layer for all computed fields. The width of the nudging layer is set equal to 15 cells along all boundaries. This value was obtained empirically for the current KASM configuration during the process of studying the behavior of the simulated fields in the vicinity of the open boundaries for the presence of artifactual high-frequency oscillations formed during the inevitable partial reflection of the signal from the open boundary. Boundary conditions for tidal motions are set using a spectral formulation with amplitudes and phases of the tidal harmonics calculated using the results of the external tidal models TPXO9, FES2014, and Arc2kmTM. Thus, the total current velocity set at the open lateral boundaries in KASM (Equation 1) include a non-tidal component retrieved from the three-dimensional velocity field provided by GLORYS12 and a tidal component calculated using results of the external tidal models. The total three-dimensional current velocity U normal to the boundary specified at the open lateral boundaries of the KASM model is calculated as follows:

$$U = U_{\text{non-tidal}} + \sum_{i=1}^{n} f_i U_{0i} \cos(\omega_i t + (v_0 + u)_i - g_i), \quad (1)$$

where n is the total number of tidal components taken into account; i is the index of a tidal component; $U_{\text{non-tidal}}$ is the three-dimensional non-tidal current velocity normal to the boundary taken from the GLORYS12 reanalysis (m/s); U_{0i} is the velocity amplitude of a tidal component normal to the boundary (m/s); $\omega_i = 2\pi/T_i$ is the wave angular velocity (rad/s); T_i is the tidal wave period (s); t is time (s); g_i is the wave phase (rad); f_i is the astronomical reduction factor; $(v_0 + u)_i$ is the astronomical argument (rad). The reduction factors and astronomical arguments for Equation 1 are calculated using a KASM module based on the UTide package [*Codiga*, 2024].

Atmospheric forcing is set using the hourly-mean data of the ERA5 reanalysis. River runoff is specified for the main rivers flowing into the Kara Sea, namely Ob, Nadym, Yenisey, Pur, Taz, Pyasina, and Taymyra, using the daily-mean discharge taken from the Global Flood Awareness System [*Grimaldi et al.*, 2022].

2.4. Description of Numerical Experiments

As a first step, a model spin-up is carried out. For this purpose, KASM is integrated for the period from January 2012 to July 2015 with boundary conditions that do not account for the tidal component in the current velocities, i.e., the current velocities at the open boundaries are set based on the daily-mean GLORYS12 reanalysis data only, thus only $U_{\text{non-tidal}}$ is taken into account in Equation (1). Subsequently, starting from August 2015, additional tidal forcing is included by introducing the tidal component of the current velocities at the open boundaries. This is achieved by calculating the normal to the boundary component of the tidal velocity for seven harmonics (M2, S2, N2, K2, K1, O1, P1) based on data from the TPXO9, FES2014, and Arc2kmTM archives. The choice of these tidal harmonics is based on an assessment of the contribution of individual tidal components to the total tide in the Kara Sea. This assessment was carried out using the data from the TPXO9 tidal model for the entire KASM domain due to an insufficient number of coastal gauges with in-situ data that would provide a long series of tidal harmonics indicating their contribution to the total tide throughout the domain. Based on this analysis, the main contribution, amounting to over 99% of tidal energy, is made by harmonics M2, S2, N2, K2, K1, O1, and P1. The contribution of harmonic Q1 is only about 0.04% of the total tidal energy, and therefore this harmonic is not taken into account in KASM. Thus, three different simulations with KASM have been carried out for the period from August to September 2015, which is mostly ice-free. In other words, each KASM experiment differs only by the source of external data used to specify the tidal component of the current velocities at the open boundaries, all other parameters being the same. These simulations will henceforth be referred to as KASM(TPXO), KASM(FES), and KASM(Arc2km). It should be noted that only the calculation results obtained for September 2015 are subjected to further harmonic analysis, while August 2015 serves as the adaptation time for the tidal forcing. The obtained hourly series of simulated three-dimensional total current velocities in the KASM domain are further depth-averaged and analyzed using the UTide package in order to determine the amplitudes and phases of individual tidal wave components simulated with KASM.

2.5. Comparison Methodology

We have compared all available data described above with each other and with available tidal observations from coastal stations in the Kara Sea. The comparison is based on the characteristics of the principal lunar semi-diurnal harmonic M2, which is the dominant tidal component in the Kara Sea [*Voinov*, 1999], and of the most significant waves: S2, K1, and O1 (Figure 2). The potential and kinetic energy (E_p and E_k) of the tidal constituents, averaged over a tidal cycle and integrated over the KASM's domain, are calculated for each model as follows [*Nekrasov*, 1990]:

$$E_p = \frac{\rho g}{4} \sum_{j=1}^{N} H_j^2 s_j, \tag{2}$$

$$E_k = \frac{\rho}{4}\sum_{j=1}^{N}\left(U_j^2 + V_j^2\right)h_j s_j, \tag{3}$$

where N is the number of grid cells in the computational KASM domain; ρ is the constant water density equal to 1025 kg/m^3; g is the gravity acceleration (m/s^2); H_j is the amplitude of the tidal wave in the j-th cell (m); U_j and V_j are the zonal and meridional velocity amplitudes of the tidal wave in the j-th cell (m/s); h_j is the water depth in the j-th cell (m); s_j is the area of the j-th cell (m^2).

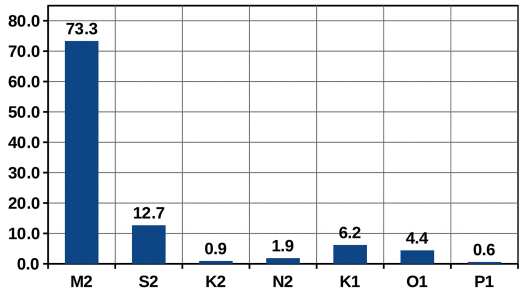

Figure 2. Individual contribution of tidal waves (in percent) to the average density of potential tidal energy in the Kara Sea based on the data from the coastal observation stations [*Hart-Davis et al.*, 2024].

To assess the quantitative differences between the modeled and observed values of tidal amplitude and phase, we utilize some widely used error metrics. The first error metric D_1 [e.g., *Kagan and Timofeev*, 2017; *Romanenkov et al.*, 2023] is computed as the average (over a tidal cycle) absolute root-mean-square vector difference between the model results and the measurements for individual tidal waves at the locations shown in Figure 1:

$$D_{1i} = \left\{\frac{1}{T}\int_0^T\left[A_{oi}\cos(\omega t - g_{oi}) - A_{mi}\cos(\omega t - g_{mi})\right]^2 dt\right\}^{1/2} = 2^{-1/2}\left[A_{oi}^2 + A_{mi}^2 - 2A_{oi}A_{mi}\cos(g_{oi} - g_{mi})\right]^{1/2}, \tag{4}$$

where A_{oi}, A_{mi}, g_{oi}, g_{mi} are the observed and modeled values of amplitude and phase of tidal sea level oscillations for an individual tidal constituent at the i-th geographical point, and T is the wave period. A somewhat similar equation was proposed by [*Janeković and Powell*, 2012], which defines the inphase-quadrature plane distance D_2:

$$D_{2i} = \sqrt{(A_{oi}\cos(g_{oi}) - A_{mi}\cos(g_{mi}))^2 + (A_{oi}\sin(g_{oi}) - A_{mi}\sin(g_{mi}))^2}. \tag{5}$$

The error metrics D_1 and D_2 account for differences in both amplitude and phase of tidal waves. We also use an absolute vector error D_{abs} to assess the total error in all points under consideration:

$$D_{(1,2)\text{abs}} = \frac{1}{n}\sum_{i=1}^{n} D_{(1,2)i}, \tag{6}$$

where n – total number of points with available measurements.

The third error metric we use in the present study is defined only in terms of amplitudes and simply is a root-mean-square error calculated as:

$$D_3 = \sqrt{\frac{1}{n}\sum_{i=1}^{n}(A_{0i} - A_{mi})^2}. \tag{7}$$

3. Results and Discussion

3.1. Comparison of External Tidal Models' Results with Each Other and with Observations

Figures 3a,b,c present the cotidal charts of the semidiurnal M2 tide based on the results of the TPXO9, FES2014, and Arc2kmTM tidal models. From Figures 3a,b it is evident that the global TPXO9 and FES2014 models yield qualitatively similar results. Differences between these two solutions are primarily observed in the M2 tidal amplitude in the northern part of the Gulf of Ob, in the Baydaratskaya Bay, and in the vicinity of Bely Island. The results of the TPXO9 model also feature a degenerate amphidromic point in the area of the Arctic Institute Islands, which is not observed in the results of the FES2014 model. In contrast to these two models, the results of the Arc2kmTM model show more pronounced sea level oscillations for the M2 wave along the southern coast of the Kara Sea, including the Gulf of Ob and the Baydaratskaya Bay. Additionally, Arc2kmTM results include a degenerate amphidromic point in the northwest of the Novaya Zemlya archipelago (Severny Island) and another amphidromic point in the Pechora Sea. In all these three solutions, an anti-clockwise rotation around an amphidromic point is present in the southwestern part of the Kara Sea, centered between the Novaya Zemlya archipelago and the Yamal Peninsula. However, a phase distribution around this amphidromic point in the Arc2kmTM model solution is slightly shifted anti-clockwise by approximately 30° compared to the results of the TPXO9 and FES2014 models.

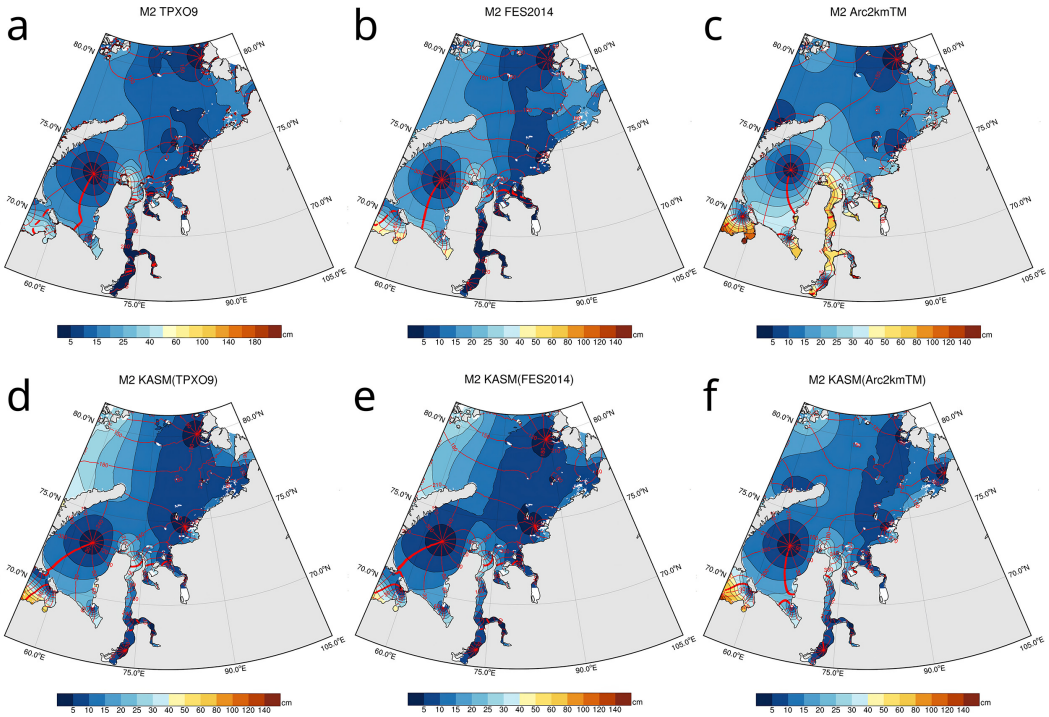

Figure 3. Cotidal charts for M2 tide based on simulations: TPXO9 – (a), FES2014 – (b), Arc2kmTM – (c), KASM(TPXO9) – (d), KASM(FES2014) – (e), KASM(Arc2kmTM) – (f). Amplitudes are indicated with color (in cm), while cotidal lines are represented with red lines (in degrees), the bold red line representing a zero phase.

Overall, having compared these M2 tidal charts with other studies, it can be concluded that the TPXO9 and FES2014 models demonstrate both qualitative and quantitative agreement with tidal charts derived from observational data [*Voinov*, 1999] as well as with those obtained from previously reported findings based on model simulations [e.g., *Kagan and Timofeev*, 2017].

In order to analyze possible causes of the differences between all the solutions presented above in the KASM's domain, we have compared the currents from the external tidal models at the open lateral boundaries, and also currents within the KASM domain

(Figure 4). Figures 4b,c show the amplitudes of the M2 barotropic tidal current velocity normal to the boundary taken from the three external tidal models. These values, along with those for other harmonics, are specified as the tidal forcing in the KASM model. At the northern boundary (Figure 4b), the velocity values are quite similar for all external models. The largest differences are demonstrated by the TPXO9 model compared to FES2014 and Arc2kmTM in the eastern part of the northern boundary off the Severnaya Zemlya archipelago. At the western boundary (Figure 4c), significant differences are observed in the Pechora Sea: 0.4, 0.7, and 1.9 m/s for TPXO9, FES2014, and Arc2kmTM, respectively. However, these differences have little effect on the behavior of the M2 wave in the Kara Sea, as it is separated from the Pechora Sea by the rather narrow Kara Gate Strait. Meanwhile, along the boundary with the Barents Sea in the northwestern part of the Kara Sea, the differences are insignificant (Figure 4c). All this demonstrates that the parameters of the M2 tidal wave coming to the Kara Sea, specified by three different external tidal models, are quite similar to each other at the open boundaries of the KASM model domain.

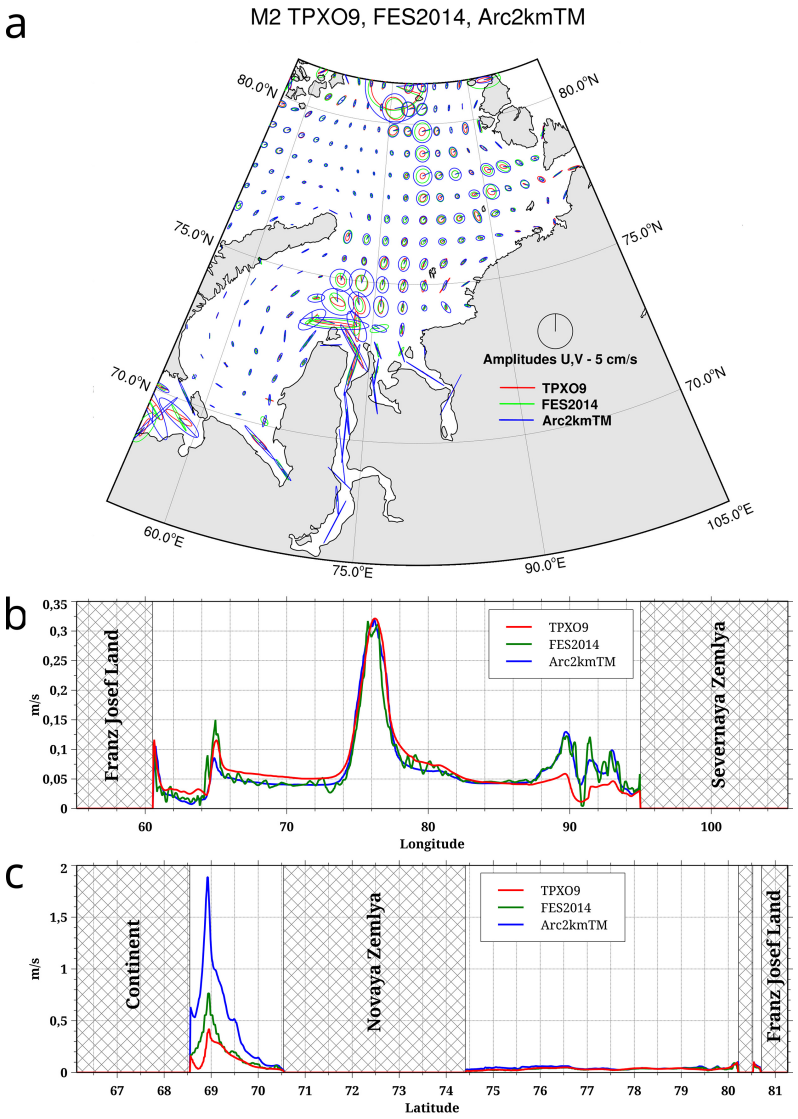

Figure 4. M2 barotropic currents in the Kara Sea as simulated by the TPXO9, FES2014, and Arc2kmTM tidal models. (a) tidal current ellipses; (b) amplitude of the tidal velocity normal to the northern boundary of the KASM domain; (c) amplitude of the tidal velocity normal to the western boundary of the KASM domain.

Differences in the solutions of the external tidal models in the KASM's domain (Figs. 3a,b,c; 4a) may be due to the different bathymetry used in these models, as well as different

Table 1. Potential and kinetic tidal energies (averaged over a tidal cycle and integrated over the KASM's domain) for the waves M2, S2, K1, and O1, calculated with Equations (2) and (3) using the results of the TPXO9, FES2014, Arc2kmTM, and KASM models. The designations KASM(TPXO9), KASM(FES2014), and KASM(Arc2kmTM) label the KASM runs forced with the corresponding tidal forcing at the open boundaries. Here E_p and E_k are expressed in TJ

	M2		S2		K1		O1	
	E_p	E_k	E_p	E_k	E_p	E_k	E_p	E_k
TPXO9	66.19	105.91	11.02	15.81	4.57	4.70	1.44	2.10
FES2014	97.78	108.98	10.99	11.64	9.53	12.36	2.38	5.82
Arc2kmTM	154.41	221.46	55.45	70.06	10.73	27.15	3.53	9.88
KASM(TPXO9)	68.63	106.85	11.64	18.70	4.22	23.62	1.06	3.57
KASM(FES2014)	48.71	87.38	5.87	11.76	4.82	33.91	1.61	4.66
KASM(Arc2kmTM)	68.36	127.19	19.48	38.26	6.07	30.96	2.09	5.19

parametrizations of turbulent exchange, bottom friction, and different spatial resolutions, since all these factors become increasingly important as the tidal wave propagates into the shallow water. In our opinion, this is the primary reason for the discrepancies between the models, but the specifics of the numerical implementation of these models, as well as differences in the data assimilation procedures, may also contribute.

As with the M2 harmonic (Figure 4a), a similar relationship generally holds for the S2, K1, and O1 harmonics: the tidal velocities simulated by the Arc2kmTM model within the KASM domain significantly exceed those obtained by the TPXO9 and FES2014 models, especially in areas with strong tidal currents, while the current velocities simulated by the TPXO9 and FES2014 models are relatively close to each other (not shown in the figures).

Some of the most powerful tidal currents in the Kara Sea are observed to the north off the Yamal Peninsula due to the tidal dynamics structure in this region. The tidal wave goes around the Yamal Peninsula clockwise, forming a false amphidromic point on Bely Island, with a corresponding velocity field nearby. Simulations of the external tidal models show that, in general, areas with higher tidal velocities also exhibit greater discrepancies between the results of these models.

We have also assessed the values of potential and kinetic tidal energies calculated using the Equations (2) and (3) for the results of all tidal models discussed herein. From Table 1 it follows that the potential and kinetic energies calculated using the Arc2kmTM model differ significantly from those obtained using the other two global models (Figure 5). This discrepancy is also corroborated in Figure 4a, which shows the tidal current ellipses for the M2 wave as obtained from the results of TPXO9, FES2014, and Arc2kmTM. It is apparent that the tidal currents simulated by the Arc2kmTM model are substantially stronger than those simulated by TPXO9 or FES2014. This difference directly leads to the correspondingly higher kinetic energy levels produced in the Arc2kmTM simulation.

Figures 6a,b,c present the absolute root-mean-square vector differences between in situ sea level measurements and model solutions produced by TPXO9, FES2014, and Arc2kmTM for M2 tide. Increased values in all three external models are reached along the coast of the northern tip of the Gydan Peninsula, as well as in the Pyasina Bay. The largest root-mean-square vector differences occur in the Arc2kmTM results along the southern coast of the Kara Sea, the absolute maximum being about two times greater than that observed in FES2014 results. An approximately similar ratio is observed in the values of absolute vector errors $D_{1\text{abs}}$ and $D_{2\text{abs}}$ (Table 2). Thus, it can be concluded that FES2014 demonstrates a more accurate solution for the Kara Sea compared to TPXO9 and Arc2kmTM as it yields the smallest errors for the most significant tidal harmonics and, therefore, can be considered as a more reliable source of information related to tidal dynamics in the Kara Sea for the purposes of regional modeling and dynamical downscaling.

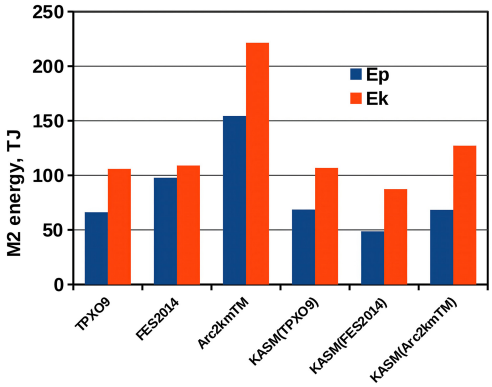

Figure 5. Potential E_p and kinetic E_k energy (averaged over a tidal cycle and integrated over the KASM's domain) of the M2 semidiurnal tide calculated using the results of the TPXO9, FES2014, Arc2kmTM, and KASM models. The designations KASM(TPXO9), KASM(FES2014), and KASM(Arc2kmTM) label the KASM runs forced with the corresponding tidal forcing at the open boundaries.

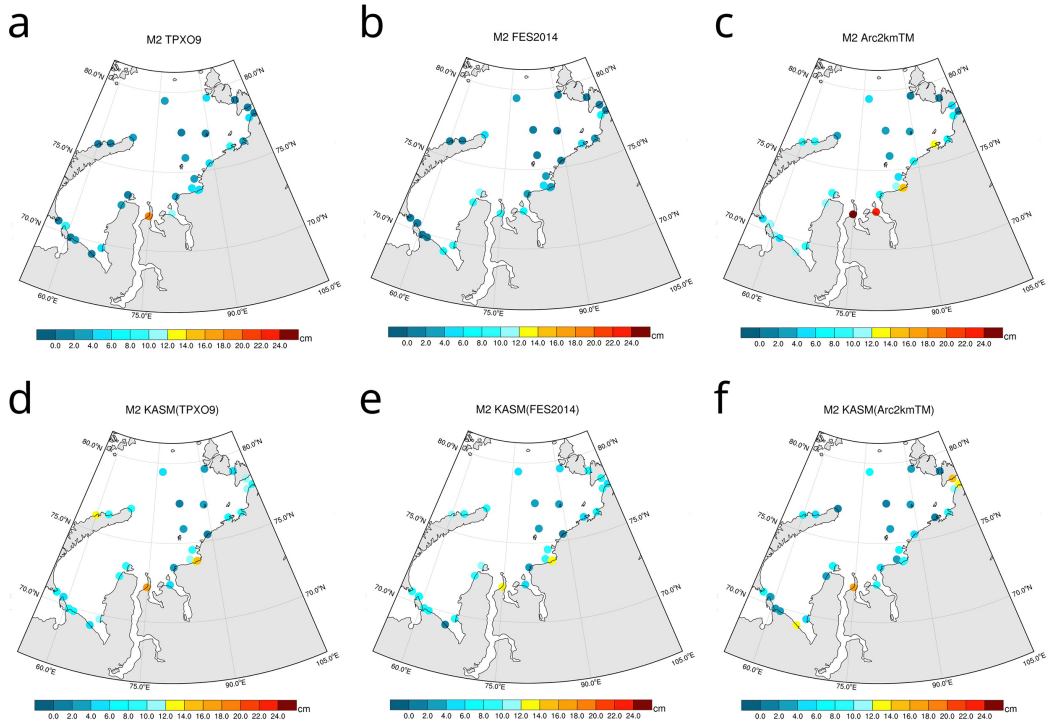

Figure 6. Average (over a tidal cycle) absolute root-mean-square vector difference between the model results and measurements for the M2 tide assessed using the Equation (4). Models: TPXO9 – (a), FES2014 – (b), Arc2kmTM – (c), KASM(TPXO9) – (d), KASM(FES2014) – (e), KASM(Arc2kmTM) – (f).

3.2. Results of KASM Simulations

As mentioned in Section 2.4, we have conducted three numerical experiments using our high-resolution regional model of the Kara Sea (KASM). In each experiment, along with the non-tidal component of currents, tidal velocities taken from the TPXO9, FES2014, or Arc2kmTM models are imposed at the open boundaries.

In the KASM(TPXO9) configuration, the model demonstrates nearly identical energy characteristics for the semidiurnal M2 and S2 tidal waves compared to the external solution (Figure 5, Table 1). Figures 3d,e present M2 cotidal charts based on the KASM(TPXO9) and KASM(FES2014) experiments and show that these two KASM solutions are largely

Table 2. Absolute errors (cm) of the models' results calculated using the Equations (4)–(7)

	M2			S2			K1			O1		
	D_{1abs}	D_{2abs}	D_3	D_{1abs}	D_{2abs}	D_3	D_{1abs}	D_{2abs}	D_3	D_{1abs}	D_{2abs}	D_3
TPXO9	4.1	5.8	6.2	2.1	3.0	2.9	1.5	2.2	1.9	1.0	1.4	1.1
FES2014	3.4	4.8	3.8	2.1	3.0	3.2	1.4	2.0	1.3	0.9	1.3	0.9
Arc2kmTM	8.6	12.2	11.7	4.9	6.9	6.2	2.2	3.1	2.0	1.4	1.9	1.5
KASM(TPXO9)	7.5	10.6	6.9	4.7	6.6	3.0	3.5	5.0	3.5	1.1	1.5	1.1
KASM(FES2014)	7.1	10.1	6.2	3.6	5.1	3.4	3.9	5.5	4.1	1.0	1.4	0.8
KASM(Arc2kmTM)	6.1	8.6	6.4	3.7	5.3	4.7	3.7	5.2	3.1	1.1	1.5	0.9

similar. However, the KASM(TPXO9) and KASM(FES2014) simulations yield slightly larger amplitudes of the M2 tidal wave in the western part of the sea, approximately up to 70°E, compared to the external solutions (Figure 3d). This is also seen in the higher values of the absolute vector errors D_{1abs} and D_{2abs} for the M2 wave presented in Table 2. We note that there is a phase shift of about 30° clockwise in the KASM(TPXO9) and KASM(FES2014) experiments relative to the external TPXO9 and FES2014 solutions in the area of the amphidromic point located in the southwestern part of the sea. This fact can possibly explain the increase in the absolute vector errors D_{1abs} and D_{2abs} for the KASM results compared to TPXO9 and FES2014, since the error calculated without considering the phase (D_3) for the KASM(TPXO9) experiment is approximately consistent with that of TPXO9: 6.9 and 6.2 cm, respectively (Table 2). Figure 3 also demonstrates that the KASM(TPXO9) and KASM(FES2014) experiments reveal an amphidromic point near the Rybny Peninsula located to the north off the Pyasina Bay, which is a degenerate amphidromic point in the TPXO9 and FES2014 simulations. Overall, KASM successfully reproduces the spatial structure of the M2 tide in the Kara Sea in both the KASM(TPXO9) and KASM(FES2014) experiments. Both solutions show six amphidromic points: in the Baydaratskaya Bay; in the southwestern part of the sea; a false amphidromic point of clockwise rotation near Bely Island; a degenerate amphidromic point located in the Yenisey Gulf; to the north off the Pyasina Bay; and the amphidromic point located to the northwest off the Severnaya Zemlya archipelago (Figures 3d,e,f). This result agrees quite well with the TPXO9 and FES2014 data, as well as with earlier independent findings reported by [*Kagan and Timofeev*, 2017], with the only difference being that [*Kagan and Timofeev*, 2017] classified the last two amphidromic points listed here as degenerate.

A somewhat different picture emerges when examining the KASM(Arc2kmTM) experiment. Although the external Arc2kmTM solution itself exhibits roughly twice the tidal energy compared to FES2014 and TPXO9 (Table 1, Figure 5), the KASM(Arc2kmTM) results show the smallest vector errors D_{1abs} and D_{2abs} for the M2 wave among all KASM experiments discussed here (Table 2). The tidal amplitudes along the coastal zone in the KASM(Arc2kmTM) experiment are noticeably lower than those in the Arc2kmTM results, and the energy of the semidiurnal M2 tide decreases by approximately twice as much (Figure 5, Table 1). Moreover, the KASM(Arc2kmTM) solution clearly reveals an additional amphidromic point located to the southwest off the entrance to the Vilkitsky Strait, which is absent in all other KASM experiments and in the TPXO9, FES2014, and Arc2kmTM data. It is noteworthy that this amphidromic point was also present in the solution obtained by [*Kagan and Timofeev*, 2017], but it was classified as a degenerate amphidromic point since its actual location was on land.

Figure 7 shows that the differences in the tidal currents simulated with the KASM model for various tidal forcings at the open lateral boundaries differ from each other to a significantly smaller degree than the solutions of the external tidal models from each other in the KASM domain (Figure 4a). Possible reasons for the significant discrepancies between the solutions of the external tidal models have been discussed earlier in the section 3.1. At the same time, as shown in Figure 4, at the open lateral boundaries, the tidal velocities taken from the external tidal models are more or less similar to each other. This leads

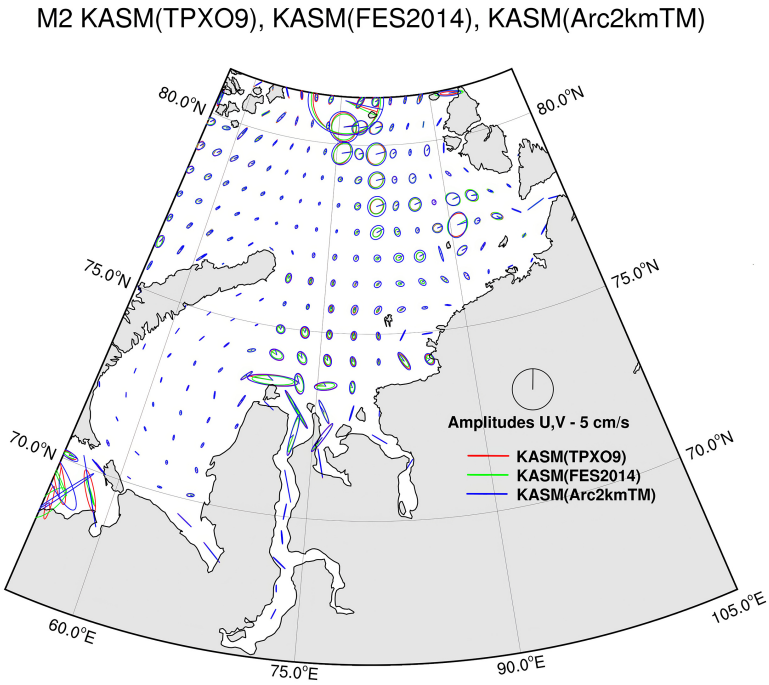

Figure 7. M2 tidal current ellipses in the Kara Sea as simulated by the KASM model forced with TPXO9, FES2014, or Arc2kmTM external tidal models at the open boundaries.

to the result that KASM yields its own solutions (i.e., KASM(TPXO9), KASM(FES2014), and KASM(Arc2kmTM)) that are significantly closer to each other than the results of the external models to each other in the inner domain, due to the fact that all other parameters, except boundary tidal forcing, are unchanged in all KASM simulations. This is also evident from the comparison of the error values presented in Table 2: the scatter of errors for KASM is smaller than for the external tidal models. The same pattern as for the M2 tidal current ellipses based on KASM results also remains for the S2, K1, and O1 harmonics: all KASM results are significantly closer to each other than the results of the three external tidal models (not shown).

Comparison of the M2 tidal charts based on the results of KASM simulations with the map based on observational data reported in [*Voinov*, 1999] suggests that the KASM(Arc2kmTM) experiment shows slightly better agreement with observations in terms of amplitudes and phases.

4. Conclusion

This study presents a comparative analysis of numerical simulations of tidal dynamics in the Kara Sea, where tidal forcing at open lateral boundaries is derived from various external tidal models. The results are compared with sea level measurements from coastal stations. The study examines the results of simulations performed using a high-resolution regional Kara Sea model (KASM) based on MITgcm, as well as results from the TPXO9, FES2014, and Arc2kmTM external tidal models.

We have assessed the tidal energy for all model solutions considered in this study. It has been found that the potential and kinetic energies computed using Arc2kmTM data differ significantly from those obtained with TPXO9 and FES2014. However, the tidal energies in all KASM solutions show smaller differences between each other compared to external tidal models.

Absolute root-mean-square vector differences have also been calculated for all model solutions using various error metrics. Overall, it can be concluded that among all the external tidal models, the solution from FES2014 yields the smallest error, followed by TPXO9, while Arc2kmTM shows the poorest agreement with observations. However, the

best-performing KASM solution is achieved when tidal forcing from Arc2kmTM is applied at the open boundaries, followed in terms of quality by KASM(FES2014), and then by KASM(TPXO9). The main errors in KASM, as inferred from comparing error metrics, arise from a slight phase shift in the tidal signal in the southwestern Kara Sea, whereas tidal amplitudes are reproduced more accurately. Differences in the solutions of the external tidal models in the KASM's domain may be due to the different bathymetry used in these models, as well as different parametrizations of turbulent exchange, bottom friction, and different spatial resolutions since all these factors become increasingly important as the tidal waves propagate into the shallow water. Additionally, different numerical implementation and assimilation techniques used in the external tidal models, may also contribute. On the contrary, KASM yields its own solutions that are significantly closer to each other than the results of the external models to each other. This is due to the fact that all other parameters, except boundary tidal forcing, are unchanged in all KASM simulations.

Summarizing this analysis of the selection of tidal forcing at the open boundaries of the regional model, we note that KASM initially was developed as a high-resolution Kara Sea model, where explicit tidal motion was not primarily intended for detailed studies of tidal dynamics but rather for explicitly accounting for tidal energy impact to various processes such as river plume formation, lens dynamics, eddy generation, accurate sea ice regime simulation, and marine biogeochemical processes. Therefore, the choice of tidal boundary forcing should be based on the best agreement in energy characteristics, particularly kinetic energy. However, validation of the model against observed tidal current velocities in the Kara Sea is a challenging task due to the lack of free publicly available observation data. Thus, the reliability of tidal current velocities, both presented in tidal atlases and in KASM, can only be assessed indirectly by comparing total kinetic energy values in the study area. In this context, the only reliable criterion for model quality assessment remains the agreement with sea level observations at coastal stations. Among the conducted numerical experiments, the smallest error has been achieved using boundary tidal forcing based on Arc2kmTM data.

Based on the analysis of all available data, including sea level measurements, tidal atlases, and our own simulations, the following conclusions can be summarized as follows:

1. Existing tidal models show significant discrepancies in estimates of total tidal energy for the Kara Sea. The FES2014 model demonstrates the best agreement with observations at coastal stations, yet the ratio of total kinetic energy to potential energy for the M2 tide differs substantially from other solutions. The Arc2kmTM model shows the poorest agreement with observations.
2. When selecting tidal boundary forcing for a regional Kara Sea model, no single atlas can be universally recommended, as various models may employ significantly different forcing methods. In KASM, tidal forcing is imposed via velocities at the open boundaries. In general, global model data, such as FES2014 and TPXO9, can be recommended for the tidal forcing for the Kara Sea.
3. KASM experiments show that Arc2kmTM forcing, which provides the smallest error when compared to coastal sea level observations, is the most suitable for our purposes, taking into account that KASM was initially developed as a tool for studying the interaction between physical and biogeochemical processes in the Kara Sea, and where the tidal mode of motion is only one of numerous factors affecting them.

Thus, the results presented in this study highlight the importance of taking into account regional conditions and specific modeling objectives when selecting tidal boundary forcing, as well as the need for further improvements in model validation methods given the limited availability of observational data.

Acknowledgments. The research was carried out within the state assignment of Ministry of Science and Higher Education of the Russian Federation for IO RAS (theme No. FMWE-2024-0028). This work used resources of the Deutsches Klimarechenzentrum (DKRZ) granted by its Scientific Steering Committee (WLA) under project ID ba1206.

References

Cai S., Long X., Liu H., et al. Tide model evaluation under different conditions // Continental Shelf Research. — 2006. — Vol. 26, no. 1. — P. 104–112. — https://doi.org/10.1016/j.csr.2005.09.004

Campin J.-M., Adcroft A., Hill C., et al. Conservation of properties in a free-surface model // Ocean Modelling. — 2004. — Vol. 6, no. 3/4. — P. 221–244. — https://doi.org/10.1016/s1463-5003(03)00009-x

Chantsev V. Y. and Danshina A. V. A calculation of the intra-annual dynamics of the Ob Bay hydrophysical regime with high spatial resolution // Fundamental and Applied Hydrophysics. — 2019. — Vol. 12, no. 3. — P. 55–64. — https://doi.org/10.7868/s2073667319030079 — (In Russian).

Codiga D. UTide Unified Tidal Analysis and Prediction Functions. — 2024. — URL: https://www.mathworks.com/matlabcentral/fileexchange/46523-utide-unified-tidal-analysis-and-prediction-functions.

Egbert G. D. and Erofeeva S. Y. Efficient Inverse Modeling of Barotropic Ocean Tides // Journal of Atmospheric and Oceanic Technology. — 2002. — Vol. 19, no. 2. — P. 183–204. — https://doi.org/10.1175/1520-0426(2002)019<0183:eimobo>2.0.co;2

Gaspar P., Grégoris Y. and Lefevre J. A simple eddy kinetic energy model for simulations of the oceanic vertical mixing: Tests at station Papa and long-term upper ocean study site // Journal of Geophysical Research: Oceans. — 1990. — Vol. 95, no. C9. — P. 16179–16193. — https://doi.org/10.1029/jc095ic09p16179

Grimaldi S., Salamon P., Disperati J., et al. River discharge and related historical data from the Global Flood Awareness System, v4.0. — European Commission, Joint Research Centre (JRC), 2022. — https://doi.org/10.24381/CDS.A4FDD6B9

Hallberg R. Using a resolution function to regulate parameterizations of oceanic mesoscale eddy effects // Ocean Modelling. — 2013. — Vol. 72. — P. 92–103. — https://doi.org/10.1016/j.ocemod.2013.08.007

Harms I. H. A numerical study of the barotropic circulation in the Barents and Kara Seas // Continental Shelf Research. — 1992. — Vol. 12, no. 9. — P. 1043–1058. — https://doi.org/10.1016/0278-4343(92)90015-c

Hart-Davis M. G., Howard S. L., Ray R. D., et al. ArcTiCA: Arctic tidal constituents atlas // Scientific Data. — 2024. — Vol. 11, no. 1. — https://doi.org/10.1038/s41597-024-03012-w

Howard S. L. and Padman L. Arc2kmTM: Arctic 2 kilometer Tide Model, 2021. — NSF Arctic Data Center, 2021. — https://doi.org/10.18739/A2PV6B79W

Jackett D. R. and McDougall T. J. Minimal Adjustment of Hydrographic Profiles to Achieve Static Stability // Journal of Atmospheric and Oceanic Technology. — 1995. — Vol. 12, no. 2. — P. 381–389. — https://doi.org/10.1175/1520-0426(1995)012<0381:maohpt>2.0.co;2

Jakobsson M., Mayer L., Coakley B., et al. The International Bathymetric Chart of the Arctic Ocean (IBCAO) Version 3.0 // Geophysical Research Letters. — 2012. — Vol. 39, no. 12. — https://doi.org/10.1029/2012gl052219

Janeković I. and Powell B. Analysis of imposing tidal dynamics to nested numerical models // Continental Shelf Research. — 2012. — Vol. 34. — P. 30–40. — https://doi.org/10.1016/j.csr.2011.11.017

Jean-Michel L., Eric G., Romain B.-B., et al. The Copernicus Global 1/12° Oceanic and Sea Ice GLORYS12 Reanalysis // Frontiers in Earth Science. — 2021. — Vol. 9. — https://doi.org/10.3389/feart.2021.698876

Kagan B. A., Sofina E. V. and Timofeev A. A. The Tidal Effect on Climatic Characteristics of the Kara Sea in the Ice-Free Period // Izvestiya, Atmospheric and Oceanic Physics. — 2019. — Vol. 55, no. 2. — P. 188–195. — https://doi.org/10.1134/s0001433819020087

Kagan B. A. and Timofeev A. A. Simulation of surface and internal semidiurnal tides in the Kara Sea // Izvestiya, Atmospheric and Oceanic Physics. — 2017. — Vol. 53, no. 2. — P. 233–241. — https://doi.org/10.1134/s0001433817020050

Kowalik Z. and Proshutinsky A. Y. The Arctic Ocean Tides // The Polar Oceans and Their Role in Shaping the Global Environment. — Washington, D. C. : American Geophysical Union, 2013. — P. 137–158. — https://doi.org/10.1029/gm085p0137

Leith C. E. Stochastic models of chaotic systems // Physica D: Nonlinear Phenomena. — 1996. — Vol. 98, no. 2–4. — P. 481–491. — https://doi.org/10.1016/0167-2789(96)00107-8

Li Q., Wu H., Yang H., et al. A numerical simulation of the generation and evolution of nonlinear internal waves across the Kara Strait // Acta Oceanologica Sinica. — 2019. — Vol. 38, no. 5. — P. 1–9. — https://doi.org/10.1007/s13131-019-1437-z

Losch M., Menemenlis D., Campin J.-M., et al. On the formulation of sea-ice models. Part 1: Effects of different solver implementations and parameterizations // Ocean Modelling. — 2010. — Vol. 33, no. 1/2. — P. 129–144. — https://doi.org/10.1016/j.ocemod.2009.12.008

Lyard F. H., Allain D. J., Cancet M., et al. FES2014 global ocean tide atlas: design and performance // Ocean Science. — 2021. — Vol. 17, no. 3. — P. 615–649. — https://doi.org/10.5194/os-17-615-2021

Marchesiello P., McWilliams J. C. and Shchepetkin A. Open boundary conditions for long-term integration of regional oceanic models // Ocean Modelling. — 2001. — Vol. 3, no. 1/2. — P. 1–20. — https://doi.org/10.1016/s1463-5003(00)00013-5

Marshall J., Adcroft A., Hill C., et al. A finite-volume, incompressible Navier Stokes model for studies of the ocean on parallel computers // Journal of Geophysical Research: Oceans. — 1997. — Vol. 102, no. C3. — P. 5753–5766. — https://doi.org/10.1029/96jc02775

Martyanov S. D. High-Resolution Modeling of the Kara Sea Dynamics and Thermohaline Structure and Assessment of the Impact of Various River Runoff Forcing in the Model // Water Resources. — 2023. — Vol. 50, S3. — S323–S327. — https://doi.org/10.1134/s0097807823700525

Martyanov S. D., Dvornikov A. Y., Gorchakov V. A., et al. Model estimates of the ecosystem contribution in the carbon dioxide exchange between the ocean and the atmosphere in the Barents Sea // Fundamental and Applied Hydrophysics. — 2017. — Vol. 10, no. 1. — P. 11–16. — https://doi.org/10.7868/S2073667317010026

Martyanov S. D., Dvornikov A. Y., Ryabchenko V. A., et al. Investigation of the relationship between primary production and sea ice in the arctic seas: assessments based on a small-component model of marine ecosystem // Fundamental and Applied Hydrophysics. — 2018. — Vol. 11, no. 2. — P. 108–117. — https://doi.org/10.7868/s2073667318020107

Mason E., Molemaker J., Shchepetkin A. F., et al. Procedures for offline grid nesting in regional ocean models // Ocean Modelling. — 2010. — Vol. 35, no. 1/2. — P. 1–15. — https://doi.org/10.1016/j.ocemod.2010.05.007

Morozov E. G., Kozlov I. E., Shchuka S. A., et al. Internal tide in the Kara Gates Strait // Oceanology. — 2017. — Vol. 57, no. 1. — P. 8–18. — https://doi.org/10.1134/s0001437017010106

Morozov E. G., Paka V. T. and Bakhanov V. V. Strong internal tides in the Kara Gates Strait // Geophysical Research Letters. — 2008. — Vol. 35, no. 16. — https://doi.org/10.1029/2008gl033804

Nekrasov A. V. Energy of ocean tides. — Leningrad : Gidrometeoizdat, 1990. — 288 p. — (In Russian).

Nguyen V. T. and Lee M. Effect of Open Boundary Conditions and Bottom Roughness on Tidal Modeling around the West Coast of Korea // Water. — 2020. — Vol. 12, no. 6. — P. 1706. — https://doi.org/10.3390/w12061706

Nurser A. J. G. and Bacon S. The Rossby radius in the Arctic Ocean // Ocean Science. — 2014. — Vol. 10, no. 6. — P. 967–975. — https://doi.org/10.5194/os-10-967-2014

Padman L. and Erofeeva S. A barotropic inverse tidal model for the Arctic Ocean // Geophysical Research Letters. — 2004. — Vol. 31, no. 2. — https://doi.org/10.1029/2003gl019003

Parkinson C. L. and Washington W. M. A large-scale numerical model of sea ice // Journal of Geophysical Research: Oceans. — 1979. — Vol. 84, no. C1. — P. 311–337. — https://doi.org/10.1029/jc084ic01p00311

Postlethwaite C. F., Morales Maqueda M. A., Fouest V. le, et al. The effect of tides on dense water formation in Arctic shelf seas // Ocean Science. — 2011. — Vol. 7, no. 2. — P. 203–217. — https://doi.org/10.5194/os-7-203-2011

Romanenkov D. A., Sofina E. V. and Rodikova A. E. Modeling of Barotropic Tide off the Southeastern Coast of the Kamchatka Peninsula in View of the Accuracy of Global Tidal Models in the Northwest Pacific Ocean //Fundamental and Applied Hydrophysics. — 2023. — Vol.16, no. 4. — P. 45–62. — https://doi.org/10.59887/2073-6673.2023.16(4)-4

Solano M., Canals M. and Leonardi S. Barotropic boundary conditions and tide forcing in split-explicit high resolution coastal ocean models // Journal of Ocean Engineering and Science. — 2020. — Vol. 5, no. 3. — P. 249–260. — https://doi.org/10.1016/j.joes.2019.12.002

Voinov G. N. Tidal phenomena in the Kara Sea. — Saint-Petersburg : Russian Geographical Society Publ., 1999. — 109 p. — (In Russian).

Voinov G. N., Golovin N. V., Kubyshkin N. V., et al. Approach to solving the problem of sea level forecasting off Cape Kamenny in the Ob' Bay // Arctic and Antarctic Research. — 2023. — Vol. 69, no. 1. — P. 29–43. — https://doi.org/10.30758/0555-2648-2023-69-1-29-43 — (In Russian).

Voinov G. N., Morozova O. A., Nesterov A. V., et al. Tides in the southern area of the Kara Sea in the vicinity of the Belyi island // Arctic and Antarctic Research. — 2020. — Vol. 66, no. 1. — P. 6–19. — https://doi.org/10.30758/0555-2648-2020-66-1-6-19 — (In Russian).

Voinov G. N. and Naumov A. K. The tides in the south-western Kara sea. Tides calibration method effects // Arctic and Antarctic Research. — 2017. — No. 4. — P. 98–115. — https://doi.org/10.30758/0555-2648-2017-0-4-98-115 — (In Russian).

Voinov G. N. and Piskun A. A. Tidal and storm surges levels variation at the Cape Kamenny (Gulf of the Ob) // Arctic and Antarctic Research. — 2019. — Vol. 65, no. 1. — P. 15–33. — https://doi.org/10.30758/0555-2648-2019-65-1-15-33 — (In Russian).

Voinov G. N. and Piskun A. A. Tidal and nontidal variations in the water level in the middle part of the Ob' Bay // Arctic and Antarctic Research. — 2023. — Vol. 69, no. 3. — P. 272–289. — https://doi.org/10.30758/0555-2648-2023-69-3-272-289 — (In Russian).